coatings

MDPI

Article

Design and Analysis of Gas Diffusion Layers in a Proton Exchange Membrane Fuel Cell

Kenan Saka [1], Mehmet Fatih Orhan [2,*] and Ahmed T. Hamada [2]

[1] Vocational School of Yenisehir Ibrahim Orhan, Bursa Uludag University, 16900 Bursa, Turkey
[2] Department of Mechanical Engineering, American University of Sharjah, Sharjah 26666, United Arab Emirates
* Correspondence: morhan@aus.edu

Abstract: A proton exchange membrane fuel cell is an energy convertor that produces environmentally friendly electrical energy by oxidation of hydrogen, with water and heat being byproducts. This study investigates the gas diffusion layer (GDL) of the membrane electrode assembly (MEA) in proton exchange membrane fuel cells (PEMFCs). In this regard, the key design concerns and restraints of the GDL have been assessed, accompanied by an inclusive evaluation of the presently existing models. In addition, the common materials used for the GDL have been explored, evaluating their properties. Moreover, a case study of step-by-step modeling for an optimal GDL has been presented. An experimental test has been carried out on a single cell under various compressions. Lastly, a parametric study has been performed considering many design parameters, such as porosity, permeability, geometrical sizes, and compression of the GDL to improve the overall efficiency of the fuel cell. The results are presented in this paper in order to help ongoing efforts to improve the efficiency of PEMFCs and facilitate their development further.

Keywords: fuel cells; proton exchange membrane; membrane electrode assembly (MEA); gas diffusion layer (GDL); permeability

Citation: Saka, K.; Orhan, M.F.; Hamada, A.T. Design and Analysis of Gas Diffusion Layers in a Proton Exchange Membrane Fuel Cell. *Coatings* **2023**, *13*, 2. https://doi.org/10.3390/coatings13010002

Academic Editor: Ioannis V. Yentekakis

Received: 17 November 2022
Revised: 9 December 2022
Accepted: 16 December 2022
Published: 20 December 2022

1. Introduction

The gas diffusion layer (GDL) is considered a crucial part of the membrane electrode assembly (MEA) because it plays several critical roles in a typical fuel cell application [1]. It acquires a porous structure with an increased surface area and is usually fabricated by weaving carbon fibers into a carbon cloth or by pressing carbon fibers into carbon paper. The GDL facilitates diffusion of reactants across the catalyst-layered membrane, provides fuel cell moisture control, and allows for heat transfer during cell operation. In addition, it is essential for GDLs to be hydrophobic and electrically conductive. Hydrophobicity ensures that the required amount of generated water at the cathode is successfully discharged to avoid water flooding [2], which can negatively affect gas diffusion, and to provide adequate humidification of the cells. Nevertheless, simultaneously enhancing electrical conductivity and hydrophobicity is challenging. This is because improving the electrical conductivity of the GDL requires high concentrations of carbon; however, this tends to result in a loss of hydrophobicity. The GDL's hydrophobicity is usually achieved by the deposition of thin films of polytetrafluoroethylene (PTFE) films or fluorinated ethylene propylene (FEP). PTFE films, for instance, are fabricated by mixing PTFE suspensions with sugar/ammonium carbonate and then heating the mixture at elevated temperatures in order to induce bubbles, which facilitate the formation of porous PTFE films [3]. FEP, on the other hand, can be deposited on carbon papers by either spraying, brushing, or dipping, with dripping being the most commonly utilized owing to the even distribution of FEP coatings and the flexibility in terms of adjusting the deposited concentrations [4]. Using this method, carbon paper is dipped in an FEP solution, excess suspensions are dropped, and specimens are dried, then placed in an oven to remove the surfactant/solvent, and

they are finally placed in a furnace and sintered in order to fix the deposited FEP layer onto the carbon paper [4].

The porous GDL in polymer electrolyte membrane fuel cells (PEMFCs) plays an important role in many crucial tasks, such as diffusing reactant gases effectively to catalyst layers and discharging liquid water. The porosity of the GDL contains macro porous substrate (10–50 μm pore sizes), generally carbon based, which provides mechanical strength, electrical conductivity, and transport for gas reactants and water product. In addition, it employs at least one micro porous layer (10–100 nm [4,5] pore sizes depending on whether PTFE/FEB coating is applied) to enhance conductivity. Generally, microporous layers are fabricated using water-based slurries that employ a thickening agent, which helps prevent the slurry from intruding into the hydrophobized porous substrate [5]. In electron transport, the main aspect is the thickness of the GDL and gas channel width, which determines the distribution of the current.

Diffusivity, porosity, size, and permeability of the GDL are other important aspects that need to be considered, as they have a substantial effect on the overall fuel cell efficiency. Therefore, there is an ongoing effort to use various methods to model GDL and design for these aspects. A bibliometric analysis by Cindrella et al. [6] shows a total of more than 400 publications since 1992, with an exponential growth, which reveals the high potential of PEMFC in the future. For instance, Litster and McLean [7] presented the design of electrodes in a PEMFC. They also performed a comparative efficiency analysis on various types of electrode. The study weighs the operating characteristics, such as temperature, pressure, and purity of the gases. In another study, Litster et al. [8] presented a computational study of heat and mass transfer in a micro-structured PEMFC cathode. Tavakoli and Weidner [9] studied the effects of contaminants on the efficiency of a PEMFC. Ohashi et al. [10] presented leakage aids for the balance of plant of PEMFCs. Jayakumar et al. [11] studied gas transport in two-layer PEMs. Roy et al. [12] investigated the efficiency of MEA for high temperature PEMFC. The details of how to design the GDLs and the MEAs were also presented, with a single cell test and its electrochemical characterizations. In addition, a parametric study was conducted on the effect of electrolyte membrane and polymer binders on the fuel cell overall efficiency and durability. A model was developed and experimentally verified by Feser et al. [13] to account for the compressibility effect when measuring permeability. The algorithm for condensation that has been presented by Alink et al. [14,15] shows that the liquid water redirects the water path in the gas diffusion layer. Liu et al. [16] studied the liquid water exchange features of porous diffusion channels in PEMFCs. Kim et al. [17] investigated lattice Boltzmann simulation of liquid water transport in the microporous and GDLs of PEMFCs. Lee et al. [18] presented a pore-network analysis of two-phase water transport in the GDLs of PEMFCs. Zamel and Li [19] explored efficient transfer properties for PEMFCs, with a focus on the GDL. Suresh and Jayanti [20] evaluated the influence of airflow on liquid water transport across a hydrophobic GDL of a PEMFC. Zamel et al. [21] studied the impact of liquid water on the transference of the GDL of PEMFCs. Sinha and Wang [22] investigated liquid water transfer in a mixed-wet GDL of a PEMFC.

The fuel cell can produce an excessive amount of water that limits the entry of reactant gases, and thus reduces the overall efficiency. Therefore, water management is a crucial task while operating a fuel cell [23]. For water management improvement, it is important to study the internal aspects and mechanism of the fuel cell to transport water, especially in the GDL, where reactants and electrons are also transported through. Water is managed by letting the correct amount of water access, and this remains at the membrane for hydration. On the other hand, hydrophobic polymers are used to avoid flooding in the GDL. To confirm that the pores of the GDL are not blocked by liquid water, a wet-proofed Teflon coating is usually used. The content of hydrophobic fluorinated ethylene propylene plays a crucial role of hydrophobicity on the surface morphology of the GDL, and their experimental results showed that the management of water improves with larger permeability and hydrophobic treatment.

The objective of this study is to provide a step-by-step detailed design process of modelling GDLs within PEMFCs to gain detailed insights into the importance of such components within the fuel cell's MEA. Even though previous work has already been conducted in this regard, the analyses presented within this study is regarded as a more accurate approach towards GDL modelling as it accounts for its electrical conductivity (commonly neglected) to enhance the accuracy of the obtained results as it can become a limiting factor based on the geometry and composition of the employed GDL. Through the developed model, a parametric study was conducted by accounting for numerous design parameters, such as porosity, permeability, and geometrical sizes to further facilitate the comprehension of GDLs and their operations. In addition, experimental tests were carried out on a single cell under various operating conditions, such as compression torques, to investigate its impacts on operating cell voltages and polarizations. This study also provides a brief overview of the various key design concerns and restraints, as well as an inclusive evaluation of the currently existing models.

2. System Description

The GDL is placed between the catalyst layer and the bipolar plates in a PEMFC, as illustrated in Figure 1. It provides an electrical connection between the electrodes and the bipolar plates and distributes reactant gases to the catalyst layers. Additionally, the GDL enables the produced water to leave the electrode surface and migrate between electrodes and flow channels. The five main functions of the GDL are as follows,

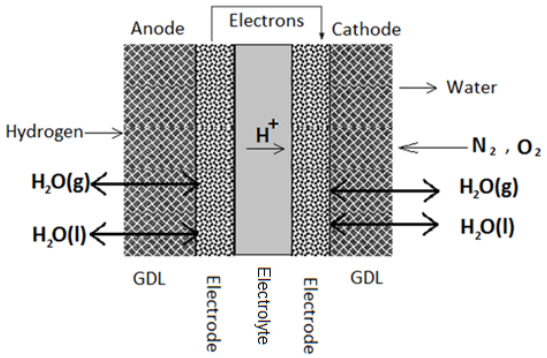

Figure 1. Membrane Electrode Assembly.

1. Electronic conductivity.
2. Mechanical strength for the PEM.
3. Permeability for the catalyst.
4. Reactant access to the catalyst layers.
5. Product removal from catalyst layers.

In order to satisfy the above functions, GDLs are made of a permeable, conductive, and durable material. As previously mentioned, the GDL can be treated with carbon and fluoropolymer (PTFE) to increase its humidification and conductance. Many GDLs are made of carbon cloth and carbon paper. The thickness of the gas diffusion layers usually varies from 0.017 to 0.4 mm, and permeability differs from 70 to 80%. Table 1 lists common carbon paper properties on the market. Carbon black and hydrophobic/adapted wettability agents are also used in the current market.

Table 1. Commercially Available Carbon Papers.

Carbon Paper	Thickness (mm)	Porosity (%)	Density (g/cm^3)
Toray TGPH 090	0.30	77	0.45
LyFlex (C332) non-pyrolized	0.33	79.5	0.37
Kureha E-715	0.35	60–80	0.35–0.40
Ballard (AvCarb P50)	0.17	-	0.28
Spectracarb 2050A-1041	0.25	60–90	0.40
SIGRACET (GDL-20BA)	0.22	83	0.29

The GDL also aids in the water management of PEMFC by allowing the correct quantity of water to reach the MEA and keep it humidified. Moreover, it also helps the produced water discharge from the cathode and prevents flooding. Because the GDL is usually porous and allows for gas transport, it is typically treated with hydrophobic polymers to help prevent overflowing and flooding.

3. Design and Analysis

The typical types of GDL models in the literature are listed in Table 2. In addition to these model analyses, GDL simulations can either be 1D, 2D, or 3D. Some common methods used to analyze mass transport in GDLs are Fick's law, Darcy's law, and Stefan–Maxwell diffusion. Ohm's law is also used for electrical conductance analysis. Additionally, flow rates, velocities, and pressure drops across the GDL layers can also be accurately computed using appropriate mathematical formulations such as those presented in this section. It is important to note that, accurately modelling GDL mandates regarding the flow as a two-phase flow in order to facilitate the computation of humidity levels, gas transportation and flooding occurrences within the MEA and their effect on its operational efficiency.

Table 2. Types of Gas Diffusion Layer models investigated in the literature.

Type of Model	Description
Gas phase models	Gas phase models assume that there is only the gas phase flow in the GDL.
Liquid phase models	Liquid phase models assume that there is only the liquid phase flow in the GDL.
Two-phase flow models	Two-phase flow models describe how gas and liquid interact in a porous medium.
1-dimensional model of the GDL	Cell efficiency as a function of GDL properties
Water transport in GDL	At high water transport, the ionic resistance is lower
GDL flooding	Effect of homogenous GDL flooding analyzed
Mass transfer in porous gas diffusion medium	Fraction of water-flooded pores calculated as a function of structural parameters of the porous system
Computational fluid dynamics analysis of GDL permeability	Water management is good in systems in which the permeability in at least one direction (in-plane or through-plane) is high

The porosity of the GDL is one of the most important properties and is typically between 70 and 80%. The porosity (ϵ) depends on the GDL's areal weight, the density of the solid phase, and compressed or uncompressed thickness. The porosity is given as

$$\epsilon = 1 - \frac{W_A}{\rho_{real} d}, \quad (1)$$

where W_A, ρ_{real}, and d represent the areal weight, density, and thickness, respectively. Table 3 encompasses some popular GDL brands with the aforementioned properties and porosities. In assessing the GDL electron transport capability, three parameters are commonly measured, namely, in-plane, through-plane, and contact resistances.

Table 3. GDL Manufacturers and Products (Adapted from [24]).

Company	Thickness cm	Density g/cm^3	Weight g/m^2	Porosity %	Through Plane Ohmcm	In-Plane Ohmcm
Toray	0.019–0.037	0.44–0.45	84–167	78	0.080	0.0047–0.0058
Spectracorp	0.02–0.026	0.46–0.48	92–125		2.692–7.500	0.012–0.022
Ballard	0.0172	0.28	48		0.564	
SGL Carbon	0.02–0.042	0.21–0.42	42–140	76–88	0.263–0.577	
E-TEK	0.018–0.043	0.50–0.73	90–240		0.360–0.550	
Carbon cloth	0.038	0.31	118		0.132	0.009
Fuel Cells Etc.	0.0454	0.8	~250	63		
Freudenberg	0.0115–0.029		65–150		4.5–10 (mΩ·cm^2)	0.7–1.1 (Ω)

A porous structure in general comprises a solid matrix and pore space. Due to their geometrical complexity and irregularity, the design of pore shapes must be made by standard shapes such as cubes and spheres. Once their geometry is specified, then pore surface areas and volumes are calculated easily. The volume of the pore is an important property in determining the liquid saturation (s), which is described as the ratio of liquid water volume to pore volume.

$$s = \frac{V_l}{V_{pore}}. \quad (2)$$

It is assumed that the spaces within the pores are filled with different phases. In addition, two-phase models consider liquid and gaseous phases. The density and dynamic viscosity of the two phases are the two key parameters in modeling the GDL layer. Darcy's law can be used to simulate the fluid flow across a porous medium with the following equation of density and dynamic viscosity of the phases:

$$\rho_g = \rho_g\left(p_g, c_g\right), \ \mu_g = \mu_g\left(p_g, c_g\right), \quad (3)$$

$$\rho_l = \rho_l(p_l, c_l), \ \mu_l = \mu_l(p_l, c_l), \quad (4)$$

where p_i and c_i represent the partial pressures and mass fractions of each of the phases. The pressure difference between the two phases in the pore space is defined as Capillary pressure.

$$p_c = p_l - p_g. \quad (5)$$

The capillary pressure of a cylindrical capillary tube is (assuming the geometry of the pore spaces as spherical or cylindrical in nature):

$$p_c = -\frac{2\gamma \cos\theta}{r}, \quad (6)$$

where r, θ, and ɣ are radius of the tube, contact angle, and the surface tension, respectively. It is very important to calculate p_c in order to select an appropriate material for the GDL. In most cases, saturation, s, is the major parameter in the capillarity.

Permeability is another important aspect of the GDL. It is the ability of materials to transfer materials at specific conditions and rates. While it is not certainly proportionate to porosity, they are intensely related to one other. The permeability constant (K) is highly allied with the pore void fraction (Φ). Relative permeability, denoted by k_r, is usually used to describe how one phase flows into another. Relative permeability is related to pore size distribution, fluid viscosity, and the interfacial forces between the fluids. The permeability of a fuel cell, as previously mentioned, is reliant on the type of transport within the material. In porous media, transport phenomena are classified into four main types/modes: (1) Free molecule flow, also known as Knudsen diffusion, which occurs within low density flows where the collisions between molecules of species can be ignored. The Knudsen diffusion is considered at pore radiuses less than 0.5 μm and is generally neglected because a typical GDL has pore radiuses between 0.5 and 200 μm. (2) Bulk/continuum or viscous flow in which the gas acts like a continuum fluid compelled by the pressure gradient and the impacts between molecules. (3) Ordinary diffusion where species move due to concentration, temperature, and external force gradients. (4) The molecules travel over a solid surface in the absorbed layer and named surface flow.

The Knudsen coefficient in a cylinder-shaped extended straight pore is approximated as

$$D_K = \left(\frac{2}{3}\right) r \times \sqrt{\frac{8RT}{\pi M}}, \tag{7}$$

where, r, R, T, and M are radius, the ideal gas constant, temperature, and the molar mass of the gas, respectively.

Bulk/Darcy flow is the predominant mode of transport within GDLs and occurs due to a pressure gradient. Based on Darcy's law, the pressure drop is proportional to the flow rate in a single phase flow as

$$Q = K_D \frac{A}{\mu L} \Delta P. \tag{8}$$

For a two-phase flow in porous media, Darcy's law is extended as follows:

$$u_g = k_{rg} \frac{K}{\mu_g L} \Delta P_g, \tag{9}$$

$$u_l = k_{rl} \frac{K}{\mu_l L} \Delta P_l, \tag{10}$$

where Q, K_D, μ, u, A, k_r, L, ΔP, and K are the flow rate, Darcy constant, dynamic viscosity, velocity, cross sectional area, relative permeability, length change, pressure drop, and permeability, respectively.

To ensure rigorous and thorough modeling of GDLs, several variables are imperative to account for, such as those listed in Table 4. In general, GDLs have high electrical conductivity in comparison to the membranes, thus many GDL design models neglect conductivity analysis of the GDL. Conversely, this study takes into account electrical conductivity analyses to enhance the accuracy of the obtained results as it can become a limiting factor based on geometry and composition. The conductivity of the GDL can be calculated by Ohm's law.

Table 4. Main Design Parameters in the GDL Model (Adapted from [25]).

Variable	Equation
Overall membrane water flux (N_w)	Mass balance
Gas phase component partial pressure ($P_{c,i}$)	Stefan–Maxwell
Electronic phase current density (i_1)	Ohm's law
Temperature (T)	Energy balance
Liquid pressure (P_L)	Darcy's law
Total gas pressure (p_g)	Darcy's law
Liquid saturation (S)	Saturation relation
Electronic phase potential (Φ_1)	Charge balance
Gas phase component flux ($N_{c,i}$)	Mass balance
Overall liquid water flux (N_L)	Mass balance

A combination of the four transport modes, as previously mentioned, can be utilized to model gas phase transport. Depending upon pressure differences (such as in gas channels), diffusion, convection, and/or pore size and structure, further simplifications can be conducted to simplify the conducted analyses. For instance, the conducted analysis assumed no liquid, no convection, constant pressure, and constant heat flux conditions. Consequently, this resulted in Fickian gas phase transport. This mode of transport is expressed using three main partial differential equations (PDEs) [25]:

$$\varepsilon^2 \frac{\partial^2 \overline{u}}{\partial x^2} + \frac{\partial^2 \overline{u}}{\partial y^2} = 0, \tag{11}$$

$$\varepsilon^2 \frac{\partial^2 \overline{v}}{\partial x^2} + \frac{\partial^2 \overline{v}}{\partial y^2} = 0, \tag{12}$$

$$\varepsilon^2 \frac{\partial^2 T}{\partial x^2} + \frac{\partial^2 T}{\partial y^2} = 0, \tag{13}$$

where ε, $\overline{u}$, and $\overline{v}$ are the perturbation parameter, oxygen flow concentration, and water vapor concentration, respectively. The geometrical features of the GDL are represented in Figure 2 [25]. As is evident, the GDL is 4d units long/wide and h units high. The gas flows through the portion of the channel highlighted with dashed lines at the top of the figure. The bottom of the diagram represents the catalyst side, where heat flux and water are added to the system and gas is absorbed. Half of the upper boundary is regarded as the solid cathode material, whereas the other half is an open channel. Portions where no fluxes are input into the cathode acquire Neumann boundary conditions, and portions with no liquid water acquires Drichlet boundary conditions. More information on how the aforementioned PDEs are numerically solved are represented in [25].

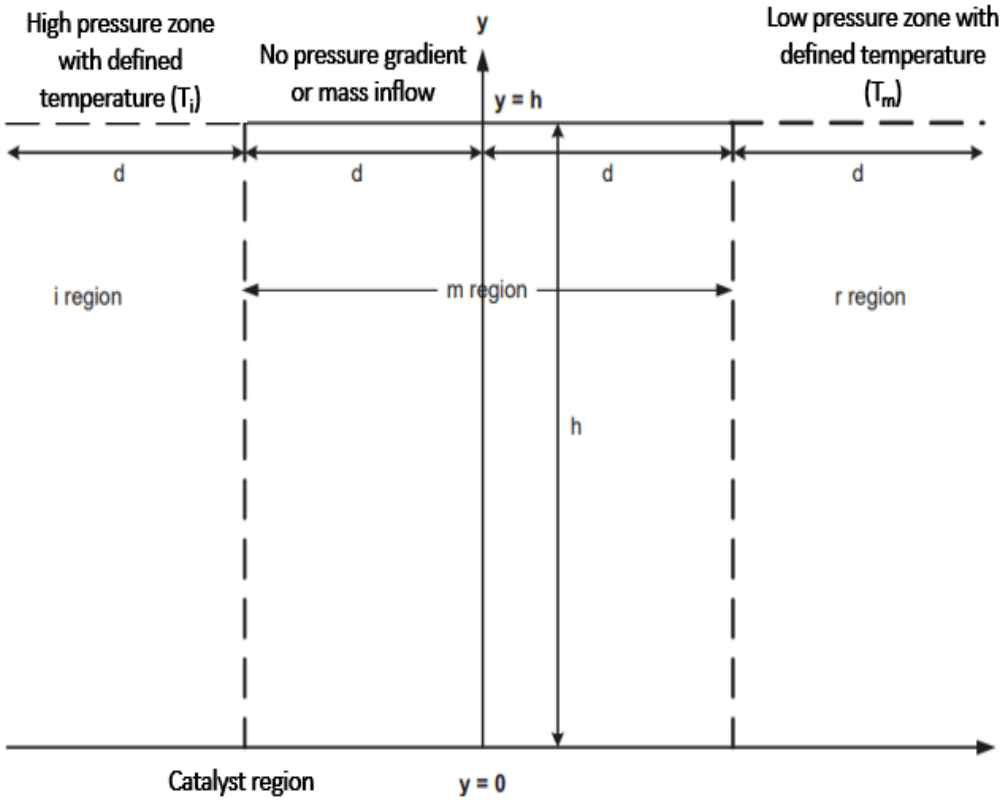

Figure 2. A simplified geometry highlighting the division of the modelled GDL (adapted from [25]).

GDL porosity, contact resistivity, liquid water fraction in pores, and the overall efficiency of the PEM fuel cell are all affected by compressing the GDL. This effect is studied here experimentally using a single cell PEM with an active surface area of 5 cm squared. Pure hydrogen and oxygen have been utilized in the tests. The cell is sealed with bolts tightened to five torque values ranging from 4 to 20 Nm. These torque values are not useful for analysis of the cell assembly. Instead, it is more beneficial to convert them to a universal measurement unit that can easily be compared across a number of assemblies. Therefore, the torque values are converted to compression force as

$$F_c = \frac{\tau N}{CD}, \tag{14}$$

where, F_c, τ, N, D, and C are the compression force, torque, the number of bolts, the nominal bolt diameter, and the friction coefficient (0.2), respectively. In this regard, using Equation (14) and associated torque values, Table 5 shows the compression forces.

Table 5. Cell Compression Values.

	Torque (Nm)	Compression Force (kN)
T1	4	43.6
T2	8	89.3
T3	12	138.1
T4	16	182.6
T5	20	221.8

4. Results and Discussion

Solving the above PDEs between $-d \leq x \leq d$ facilitates the comprehension of the Fickian gas phase transport with the GDL in terms of the variation of temperature, oxygen concentration, water vapor concentration, and saturation. The computed results are repre-

sented in the form of 2D contour plots, as shown in Figure 3. These results are utilized to justify the trends computed from the 1D model developed by this study. In other words, the PDEs are solved in a general manner, where the computed variables have no quantitative meaning but shed light on the expected output trends. Figure 3a, for instance, demonstrates a decreasing trend of temperature along the height of the GDL (positive y-axis) within the negative region of the x-axis. This is because Fickian transport assumes a constant heat flux boundary condition applied to the catalyst side and a temperature boundary condition at the top layer of the GDL [25], as shown in Figure 2, hence the decrease in temperature. This temperature trend has also been previously verified in GDLs with high in-plane electrical resistivity [26]. Physically, what happens is that the oxygen initially enters the channel with a relatively low temperature. This low temperature limits the reaction rates and consequently limits local current densities, which controls the reaction rates [26]. Therefore, the localized temperatures of the GDL at the catalyst layer take a longer time before they attains peak temperatures. In the positive region of the x-axis, the temperatures of the GDL are relatively lower, owing to the fact that oxygen (reactant) is fully consumed, thus bringing the electro-chemical reactions to a halt, and the GDL drops in temperature. The effect of temperature on the reaction rates are further highlighted in the concentration variations of oxygen (reactant) and water vapor (product), as shown in Figure 3b,c. For instance, as the temperature increases, the rate of electro-chemical reactions increase, which increases the consumption of oxygen, hence the decrease in concentration. The decrease in oxygen concentration is accompanied by an increase in the concentration of the water being produced, as evident in Figure 3c, hence the increase in saturation shown in Figure 3d. This all coincides with the 1D model of the mole fraction of oxygen and water vapor concentration in Figure 4.

In Figure 5a, the correlation between the capillary pressure and the liquid saturation level is explored. The model is based on Equation (6) and the pore network model, and it is quite accurate in predicting the relationship between the two variables. It becomes evident that the capillary pressure is indirectly related to the liquid saturation. In other words, as the capillary pressure approaches a certain breakthrough point, liquid water starts penetrating, thus leading to an increase in saturation. It is important to note that the data are only modeled for 0.1 s, because at around 0.2 s, the liquid dews penetrate over the surface, leading to distorted data being obtained. Based on the permeability equations in the earlier section, the relative permeability of the gaseous and liquid phases can be modeled accurately, as demonstrated in Figure 5b. Evidently, the relative permeability of the liquid phase exhibits an exponential growth with saturation; however, when in the gaseous phase, it exhibits an exponential decrease.

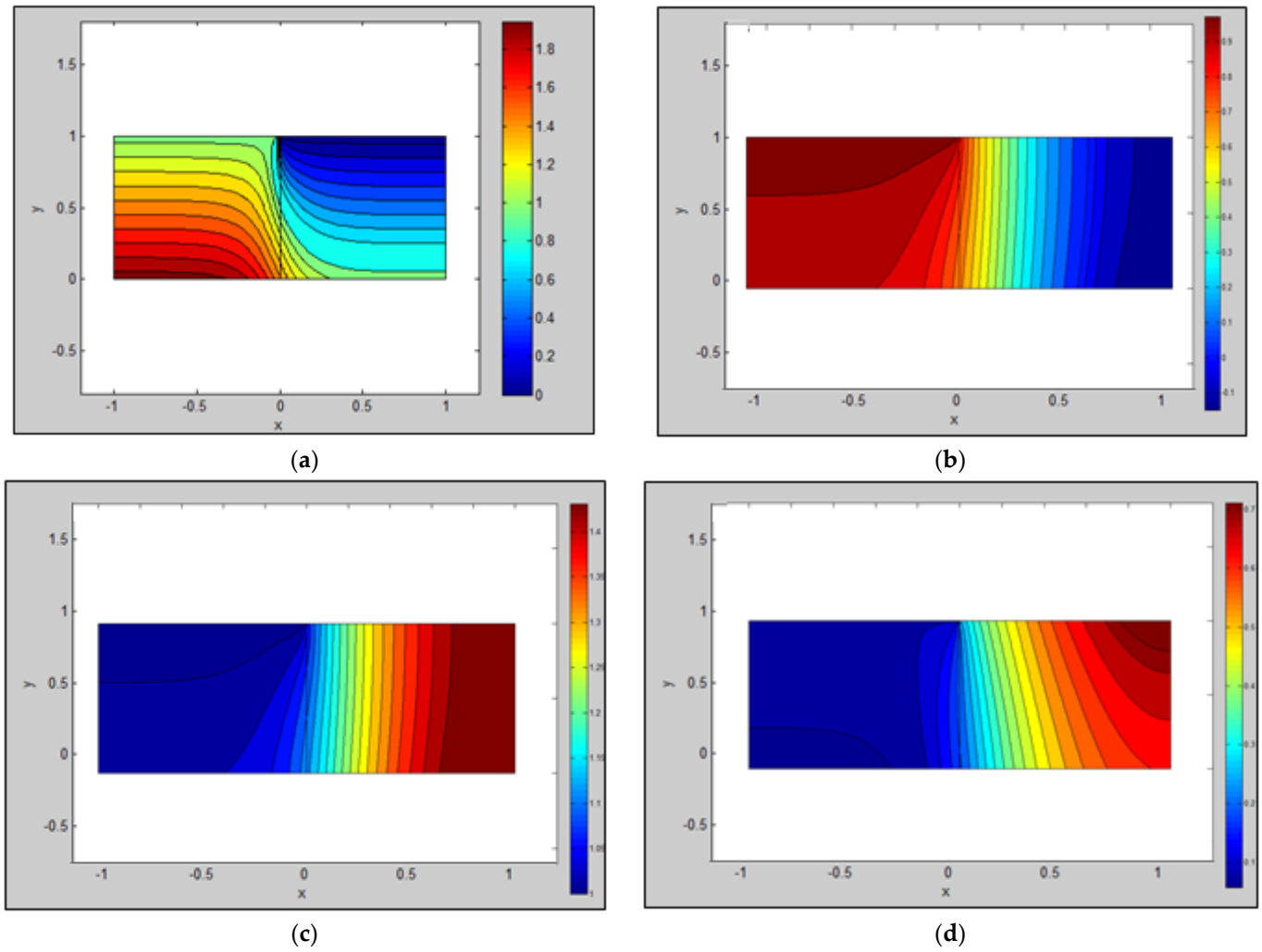

Figure 3. (**a**) Two-dimensional contour plot of temperature, (**b**) oxygen concentration, (**c**) 2D plot of water vapor concentration, (**d**) contour plot of saturation (adapted from [25]).

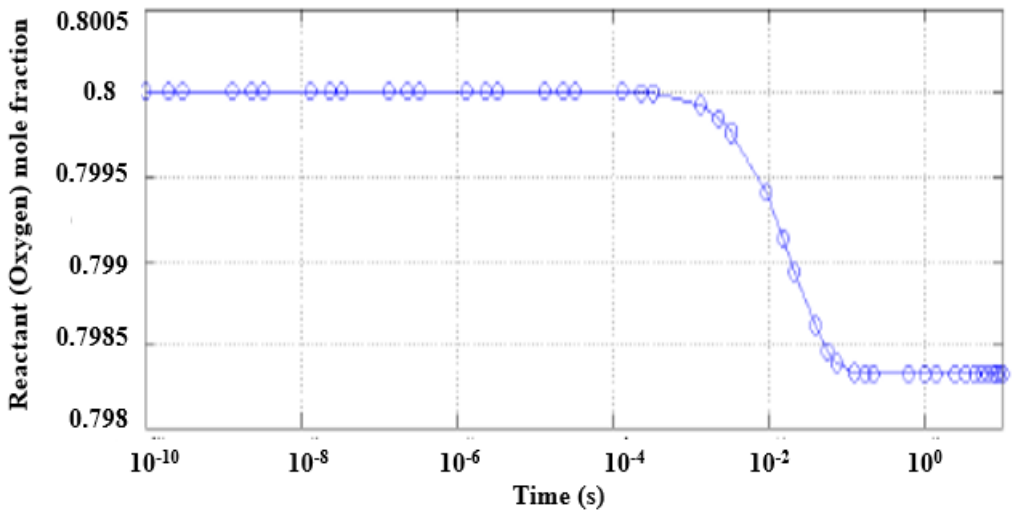

Figure 4. One-dimensional Plot of GDL reactant (oxygen) concentration.

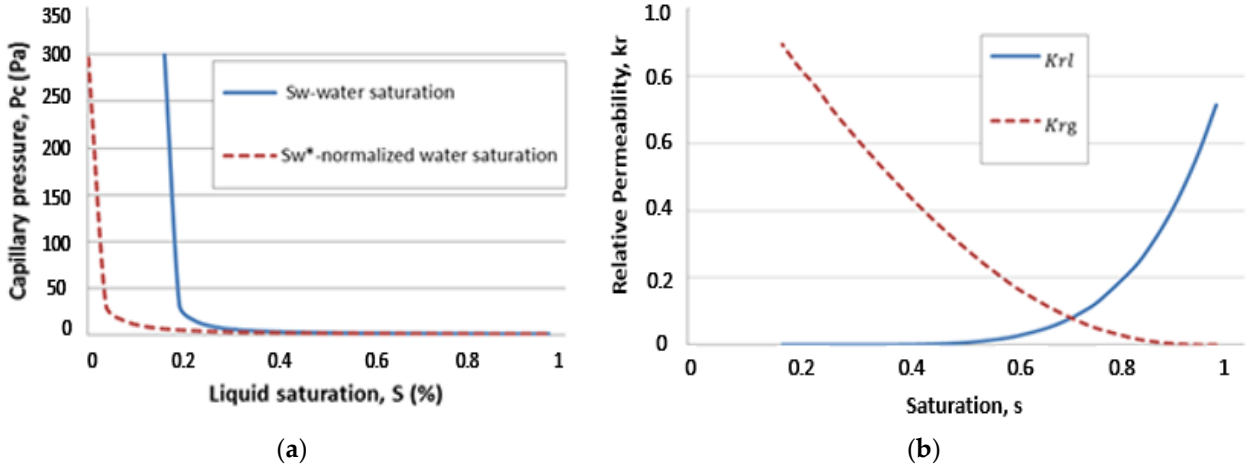

Figure 5. (**a**) Capillary pressure vs. liquid saturation, (**b**) relative permeability vs. saturation.

According to the conducted experiments and their results, the amount of compression exhibits profound effects on the overall cell performance, in particular within high current density regions. Figure 6 shows that, at intermediate current densities, increasing the compression enhances the output cell voltage, thus enhancing the overall performance of the cell. Similar trends are also obtained in [27]. This enhancement is attributed to the decrease in contact resistances as compression forces increase. Nevertheless, the cell voltage dramatically decreases beyond a certain point at high compressions. This sudden drop is attributed to the increased overpotentials at high compression torques, specifically mass transport overpotentials, as shown in Figure 7a. This is because, at increased compression, the GDL porosities decrease, thus lowering the permeability and effective diffusivity [27]. In addition, the increase in mass transport overpotentials can also be attributed to the increased amounts of water production at high current density operations. Therefore, it is essential to control the compression and determine an optimal ratio to ensure effective fuel cell operation. In addition, Figure 7b also sheds light on how the current density increases with increasing the compression torque up to 12 Nm. Beyond this value, especially at the low operating voltages, a rapid current reduction is observed. This drop is due to the reduction in the porosity of the GDL, which prevents the reactants from migrating through the catalyst layer.

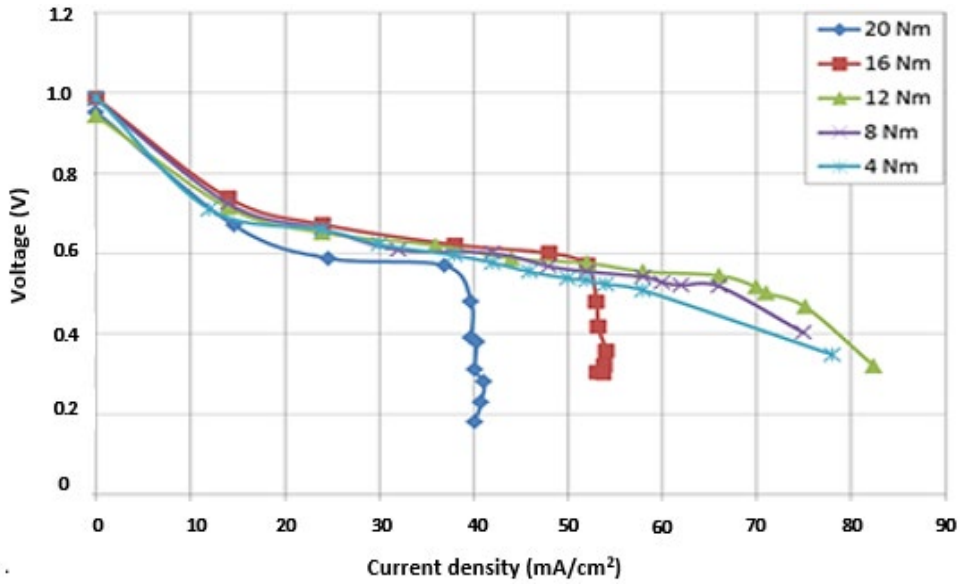

Figure 6. Polarization curves at various compression values.

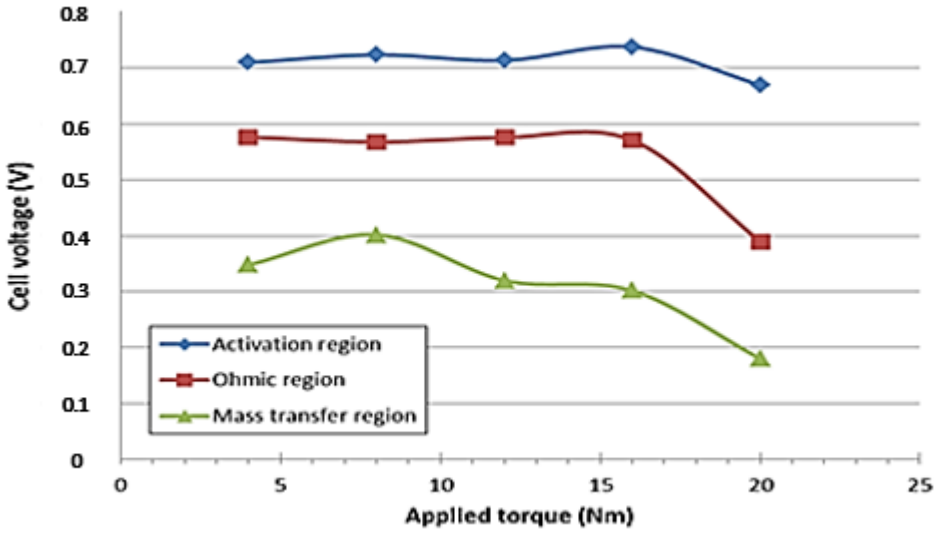

(**a**)

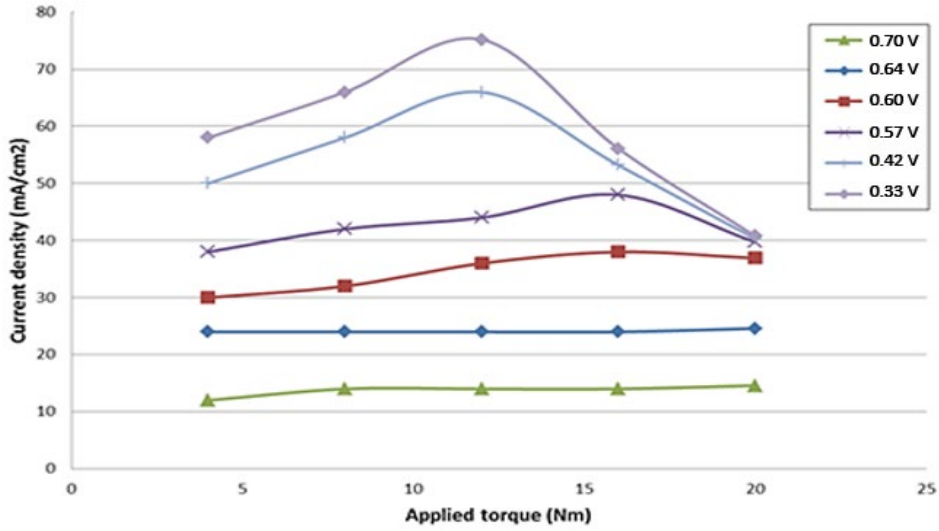

(**b**)

Figure 7. (**a**) Applied torque vs. cell voltages at the activation, ohmic, and mass transfer regions, (**b**) applied torque vs. current density at the different operating voltages.

To ensure effective operation of a PEMFC, maintaining an appropriate balance between the conductivity and permeability of the GDL layer is imperative, as suggested by Figure 8a,b, respectively. The higher the thickness being compressed, the smaller the gap between the carbon fibers and the lower the GDL porosities. Consequently, this means that there are a lower number of available three-phase reaction sites, thus decreasing the overall permeability of the GDL. The obtained results also coincide with what is available in the literature, such as in [28–30], where it has also been deduced that increased compression ratios decrease the GDL's permeability. As per the conductivity of the GDL, results have shown that increased compressions are associated with (low GDL thicknesses) with decreased conductivities, both in-plane and through-plane. Generally, increased compressions result in increased conductivities; however, this depends on many parameters (e.g., the type of carbon paper used to make up the GDL and the size of the porosities within these structures), hence the variation in trends.

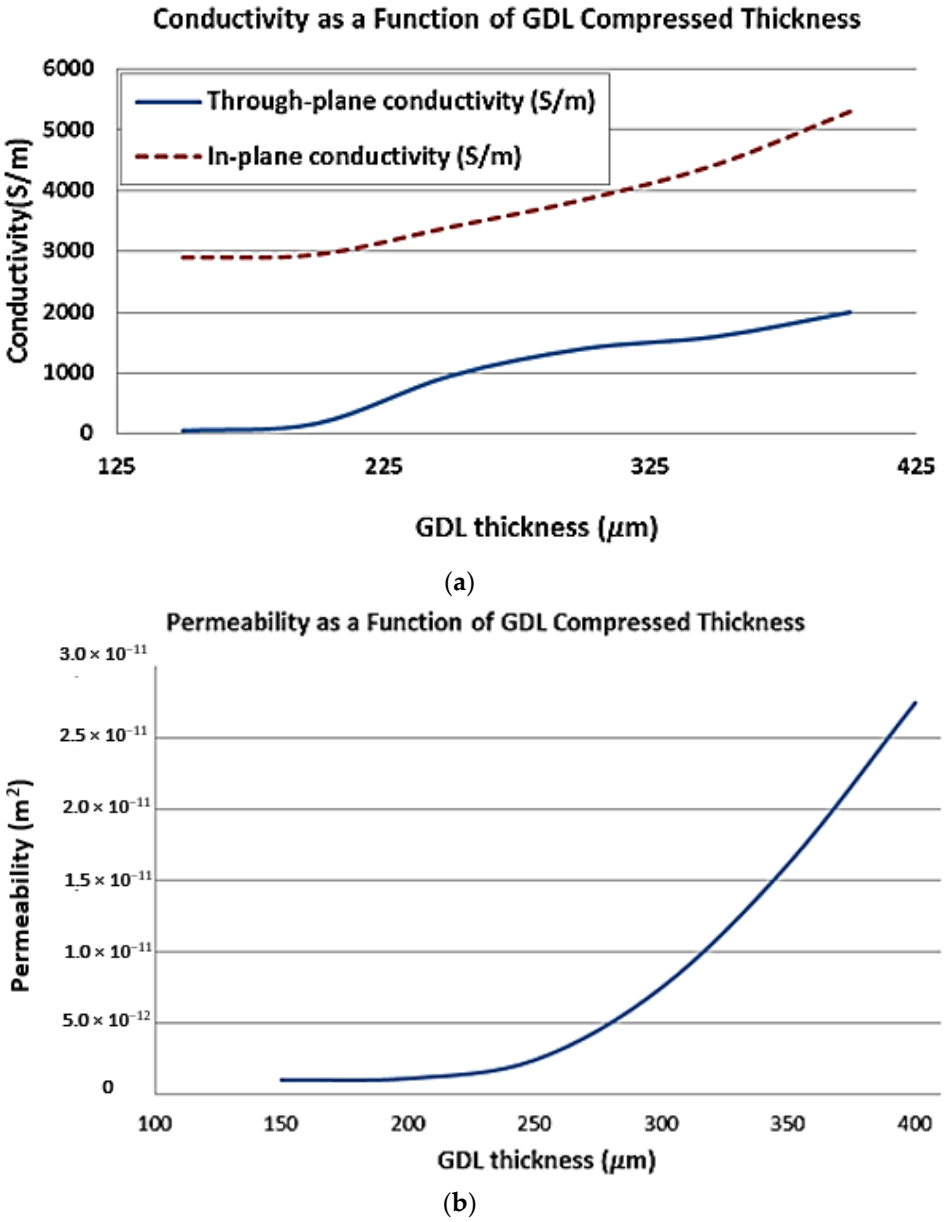

Figure 8. (**a**) Conductivity as a function of GDL compressed thickness, and (**b**) permeability as a function of GDL compressed thickness.

5. Conclusions

This study provided a step-by-step design process for a PEMFC GDL and determined its optimal operating conditions with the aid of both experimental and numerical case studies. To provide more detailed insights, a parametric study taking into account various design parameters such as porosity, permeability, geometrical sizes, and compression of the GDL was conducted in order to improve the overall efficiency of the fuel cell. Based on the obtained results, numerous deductions can be drawn from this study. For instance, a decrease in the operating temperature was observed along the direction of the reaction (positive x-direction) due to the initial release of energy at the electrode and the subsequent decrease that followed after. In addition, oxygen concentrations decreased in the direction of the reaction due to the oxygen reacting with ions and electrons at the cathode to produce water vapor. Consequently, this resulted in increased water vapor concentration and saturation rates in the positive x-direction. Results have also shown that there exists an indirect relation between the capillary pressure and liquid saturation. As the capillary

pressure approaches a certain breakthrough point, liquid water penetrates, leading to an increase in saturation. This increased saturation results in increased relative permeability; however, this is only during the liquid phase. The effect of compression on the GDL has also been investigated. It was shown that, at high current densities, increasing the compression initially increases the overall efficiency; however, beyond a certain point, further increasing the compression dramatically decreased the efficiency. In addition, the effect of compression on the polarization curve is negligible at the activation region, but it becomes substantial at the high current density values (ohmic and mass transport regions). The current density increases with increasing compression torque up to 12 Nm. Beyond this value, especially at the low operating voltages, a rapid current reduction is observed due to the reduction in the porosity of the GDL, which limits the reactants entering the catalyst layer. Due to the large amount of water generation at high current density conditions, a sharp efficiency decrease is observed in the mass transfer region compared to the ohmic and activation regions.

Author Contributions: Conceptualization and methodology, K.S. and M.F.O.; software, K.S. and M.F.O.; formal analysis, K.S.; investigation, K.S. and M.F.O.; resources, K.S. and M.F.O.; data curation, K.S. and M.F.O.; writing—original draft preparation, K.S. and M.F.O.; writing—review and editing, K.S., M.F.O. and A.T.H.; visualization, K.S., M.F.O. and A.T.H. All authors have read and agreed to the published version of the manuscript.

Funding: This research received no external funding.

Institutional Review Board Statement: Not applicable.

Informed Consent Statement: Not applicable.

Data Availability Statement: All data were mentioned in this paper. No external supporting data are available.

Acknowledgments: The work in this paper was supported, in part, by the Open Access Program from the American University of Sharjah. This paper represents the opinions of the authors and does not mean to represent the position or opinions of the American University of Sharjah.

Conflicts of Interest: The authors declare no conflict of interest.

Nomenclature

A	Surface Area (m^2)
$c_{g,i}$	Mass fraction of gas/liquid phase
C	Friction coefficient
D_K	Knudsen coefficient
D	Nominal bolt diameter (m)
F_c	Compression force (N)
i	Current Density (A cm^{-2})
K	Permeability
K_r	Relative permeability
K_D	Darcy's constant
L	Length (m)
M	Molar mass (g mol^{-1})
N	Number of bolts
P_c	Capillary pressure (Pa)
$P_{g/i}$	Partial pressure of gas/liquid phase (Pa)
$\Delta P_{g,l}$	Pressure drop of gas/liquid phase (Pa)
Q	Volume flowrate (m^3 s^{-1})
r	Radius (m)
R	Ideal gas constant (J K^{-1} mol^{-1})
s	Liquid saturation
t	Thickness (m)

T	Temperature (K)
$u_{g,l}$	Velocity of gas/liquid phase (m s^{-1})
$\overline{u}$	Oxygen concentration (mol/m^3)
V_l	Volume of liquid (m^3)
V_{pore}	Volume of pore (m^3)
$\overline{v}$	Water vapor concentration (mol/m^3)
W_A	Areal weight (kg m^{-2})
ρ_{real}	Density of solid phase (kg m^{-3})
$\rho_{g/l}$	Denity of gas/liquid phase (kg m^{-3})
ϵ	Porosity
θ	Contact angle (rad)
ɣ	Surface tension (N m^{-1})
$\mu_{g,l}$	Dynamic viscosity of gas/liquid phase (Pa s)
τ	Torque (N m)

References

1. Sharaf, O.Z.; Orhan, M.F. An overview of fuel cell technology: Fundamentals and applications. *Renew. Sustain. Energy Rev.* **2014**, *32*, 810–853. [CrossRef]
2. Wittstadt, U.; Wagner, E.; Jungmann, T. Membrane electrode assemblies for unitised regenerative polymer electrolyte fuel cells. *J. Power Sources* **2005**, *145*, 555–562. [CrossRef]
3. Gouérec, P.; Poletto, L.; Denizot, J.; Sanchez-Cortezon, E.; Miners, J.H. The evolution of the performance of alkaline fuel cells with circulating electrolyte. *J. Power Sources* **2004**, *129*, 193–204. [CrossRef]
4. Yang, T.-F.; Hsueh, C.-Y.; Chen, B.-L.; Li, W.-K.; Yan, W.-M. Effects of fluorinated ethylene propylene contents in a novel gas diffusion layer on cell performance of a proton exchange membrane fuel cell. *Int. J. Energy Res.* **2022**, *46*, 1553–1564. [CrossRef]
5. Stampino, P.G.; Cristiani, C.; Dotelli, G.; Omati, L.; Zampori, L.; Pelosato, R.; Guilizzoni, M. Effect of different substrates, inks composition and rheology on coating deposition of microporous layer (MPL) for PEM-FCs. *Catal. Today* **2009**, *147*, S30–S35. [CrossRef]
6. Cindrella, L.; Kannan, A.M.; Lin, J.F.; Saminathan, K.; Ho, Y.; Lin, C.W.; Wertz, J. Gas diffusion layer for proton exchange membrane fuel cells—A review. *J. Power Sources* **2009**, *194*, 146–160. [CrossRef]
7. Litster, S.; McLean, G. PEM fuel cell electrodes. *J. Power Source* **2004**, *130*, 61–76. [CrossRef]
8. Litster, S.; Pharoah, J.G.; McLean, G.; Djilali, N. Computational analysis of heat and mass transfer in a micro-structured PEMFC cathode. *J. Power Sources* **2006**, *156*, 334–344. [CrossRef]
9. Tavakoli, B.; Weidner, J.W. Effect of contaminants on the performance of a proton exchange membrane fuel cell. *ECS Trans.* **2015**, *66*, 77–90. [CrossRef]
10. Ohashi, M.; Weidner, J.W.; Zee, J.W.V.; Dinh, H.N. Leaching studies of assembly aids for balance of plant of PEM fuel cells. In Proceedings of the 224th ECS Meeting, San Francisco, CA, USA, 27–28 October 2013.
11. Jayakumar, J.V.; Staser, J.; Kim, C.-H.; Stone, S.G.; Weidner, J.W. Gas transport in two-layer proton exchange membranes. *ECS Trans.* **2013**, *45*, 41–53. [CrossRef]
12. Roy, A.; Hickner, M.A.; Lane, O.; McGrath, J.E. Investigation of membrane electrode assembly (MEA) processing parameters on performance for wholly aromatic hydrocarbon-based proton exchange membranes. *J. Power Sources* **2009**, *191*, 550–554. [CrossRef]
13. Feser, J.P.; Prasad, A.K.; Advani, S.G. Experimental characterization of in-plane permeability of gas diffusion layers. *J. Power Sources* **2006**, *162*, 1226–1231. [CrossRef]
14. Alink, R.; Haußmann, J.; Markötter, H.; Schwager, M.; Manke, I.; Gerteisen, D. The influence of porous transport layer modifications on the water management in polymer electrolyte membrane fuel cells. *J. Power Sources* **2013**, *233*, 358–368. [CrossRef]
15. Alink, R.; Gerteisen, D.; Oszcipok, M. Degradation effects in polymer electrolyte membrane fuel cell stacks by sub-zero operation—An in situ and ex situ analysis. *J. Power Sources* **2008**, *182*, 175–187. [CrossRef]
16. Liu, X.; Peng, F.; Lou, G.; Wen, Z. Liquid water transport characteristics of porous diffusion media in polymer electrolyte membrane fuel cells: A review. *J. Power Sources* **2015**, *299*, 85–96. [CrossRef]
17. Kim, K.N.; Kang, J.H.; Lee, S.G.; Nam, J.H.; Kim, C.-J. Lattice Boltzmann simulation of liquid water transport in microporous and gas diffusion layers of polymer electrolyte membrane fuel cells. *J. Power Sources* **2015**, *278*, 703–717. [CrossRef]
18. Lee, K.-J.; Nam, J.H.; Kim, C.-J. Pore-network analysis of two-phase water transport in gas diffusion layers of polymer electrolyte membrane fuel cells. *Electrochim. Acta* **2009**, *54*, 1166–1176. [CrossRef]
19. Zamel, N.; Li, X. Effective transport properties for polymer electrolyte membrane fuel cells—With a focus on the gas diffusion layer. *Prog. Energy Combust. Sci.* **2013**, *39*, 111–146. [CrossRef]
20. Suresh, P.V.; Jayanti, S. Effect of air flow on liquid water transport through a hydrophobic gas diffusion layer of a polymer electrolyte membrane fuel cell. *Int. J. Hydrog. Energy* **2010**, *35*, 6872–6886. [CrossRef]
21. Zamel, N.; Li, X.; Becker, J.; Wiegmann, A. Effect of liquid water on transport properties of the gas diffusion layer of polymer electrolyte membrane fuel cells. *Int. J. Hydrog. Energy* **2011**, *36*, 5466–5478. [CrossRef]

22. Sinha, P.K.; Wang, C.-Y. Liquid water transport in a mixed-wet gas diffusion layer of a polymer electrolyte fuel cell. *Chem. Eng. Sci.* **2008**, *63*, 1081–1091. [CrossRef]
23. Ijaodola, O.S.; El-Hassan, Z.; Ogungbemi, E.; Khatib, F.N.; Wilberforce, T.; Thompspn, J.; Olabi, A.G. Energy efficiency improvements by investigating the water flooding management on proton exchange membrane fuel cell (PEMFC). *Energy* **2019**, *179*, 246–267. [CrossRef]
24. Barbir, F. *PEM Fuel Cells: Theory and Practice*; Elsevier Academic Press: New York, NY, USA, 2005.
25. Spiegel, C. Chapter 8—Modeling the Gas Diffusion Layers. In *PEM Fuel Cell Modeling and Simulation Using Matlab*; Spiegel, C., Ed.; Academic Press: Burlington, NJ, USA, 2008; pp. 197–241.
26. Bapat, C.J.; Thynell, S.T. Effect of anisotropic electrical resistivity of gas diffusion layers (GDLs) on current density and temperature distribution in a Polymer Electrolyte Membrane (PEM) fuel cell. *J. Power Sources* **2008**, *185*, 428–432. [CrossRef]
27. Yan, X.; Lin, C.; Zheng, Z.; Chen, J.; Wei, G.; Zhang, J. Effect of clamping pressure on liquid-cooled PEMFC stack performance considering inhomogeneous gas diffusion layer compression. *Appl. Energy* **2020**, *258*, 114073. [CrossRef]
28. Bao, Z.; Li, Y.; Zhou, X.; Gao, F.; Du, Q.; Jiao, K. Transport properties of gas diffusion layer of proton exchange membrane fuel cells: Effects of compression. *Int. J. Heat Mass Transf.* **2021**, *178*, 121608. [CrossRef]
29. Zhu, L.; Zhang, H.; Xiao, L.; Bazylak, A.; Gao, X.; Sui, P.-C. Pore-scale modeling of gas diffusion layers: Effects of compression on transport properties. *J. Power Sources* **2021**, *496*, 229822. [CrossRef]
30. Zamel, N.; Li, X.; Shen, J. Numerical estimation of the effective electrical conductivity in carbon paper diffusion media. *Appl. Energy* **2012**, *93*, 39–44. [CrossRef]